

Polarization-controlled tunable directional spin-driven photocurrents in a magnetic metamaterial with threefold rotational symmetry

Received: 20 May 2022

Accepted: 21 October 2022

Published online: 07 November 2022

 Check for updates

Masakazu Matsubara^{1,2}✉, Takatsugu Kobayashi¹, Hikaru Watanabe³,
Youichi Yanase^{4,5}, Satoshi Iwata⁶ & Takeshi Kato⁶

Future spintronics and quantum technologies will require a portfolio of techniques for manipulating electron spins in functional nanodevices. Especially, the establishment of the methods to control spin current is the key ingredient essential for the transfer and processing of information, enabling faster and low-energy operation. However, a universal method for manipulating spin currents with full-directional controllability and tunable magnitude has not been established. Here we show that an artificial material called a magnetic metamaterial (MM), which possesses a novel spintronic functionality not exhibited by the original substance, generates photo-driven ultrafast spin currents at room temperature via the magneto-photogalvanic effect. By tuning the polarization state of the excitation light, these spin currents can be directed with tunable magnitude along an arbitrary direction in the two-dimensional plane of the MM. This new concept may guide the design and creation of artificially engineered opto-spintronic functionalities beyond the limitations of conventional material science.

Manipulation of electron spin polarization is an essential topic of spintronics^{1–3}. An attractive approach to generating and controlling spin currents is the use of light, and new principles of light conversion into spin currents have been explored, including a light-helicity-dependent control of spin-polarized currents in semiconductors⁴ and topological insulators^{5,6}, laser-generated superdiffusive spin currents in magnetic multilayers⁷, propagation control of spin waves in a magnetic insulator⁸, generation of pure spin currents by optical quantum interference effect⁹ and surface plasmon excitation¹⁰, and spin-dependent scattering^{11,12}. In the last of these techniques, pure spin currents are converted into spin-polarized DC electric currents under an applied magnetic field, generating the magneto-photogalvanic

effect (MPGE)^{13–15}. However, a universal method for manipulating spin currents with full-directional controllability and tunable magnitude, independent of specific material properties and not limited to low-temperature operation, has not been established.

Advances in nanofabrication technology can overcome the fundamental limitations imposed by nature. Metamaterials are engineered artificial materials that elicit new responses, not exhibited by the original substance, using tailored subwavelength structures¹⁶. The required material functionality can be achieved by designing the shape, size, period, and mutual arrangement of the constituent nanostructures. This deceptively simple yet powerful concept enables the realization of many unprecedented optical properties such as

¹Department of Physics, Tohoku University, Sendai 980-8578, Japan. ²Center for Science and Innovation in Spintronics, Tohoku University, Sendai 980-8577, Japan. ³Research Center for Advanced Science and Technology, University of Tokyo, Tokyo 153-8904, Japan. ⁴Department of Physics, Graduate School of Science, Kyoto University, Kyoto 606-8502, Japan. ⁵Institute for Molecular Science, Okazaki 444-8585, Japan. ⁶Institute of Materials and Systems for Sustainability, Nagoya University, Furo-cho, Chikusa-ku, Nagoya 464-8603, Japan. ✉ e-mail: m-matsubara@tohoku.ac.jp

negative refractive index¹⁷, super-resolution imaging¹⁸, cloaking¹⁹ and perfect absorption of electromagnetic waves²⁰.

During the past 20 years, metamaterials have entered the realm of nonlinear optics²¹. Especially, the introduction of noncentrosymmetry enables second-order nonlinear optical effects such as second harmonic generation (SHG), which requires, in the leading order, the breaking of space inversion symmetry. Consequently, nonlinear optical processes forbidden in centrosymmetric media are allowable in metamaterials²². The introduction of magnetism into noncentrosymmetric metamaterials causes attractive magneto-optical responses such as magnetic-field controllable SHG^{23,24} and nonreciprocal optical magnetoelectric effect²⁵, originating from the breaking of both space inversion and time-reversal symmetries. The MPGE, which are used in this study as the principle of photo-driven ultrafast spin current generation, can be allowed under the same conditions. The MPGE (called the magnetic ratchet effect in artificial periodic structures) has been detected in metamaterials with nonmagnetic superlattices^{26,27}. However, it has never been observed in magnetic metamaterials (MMs).

In this study, we report the observation of MPGE in non-centrosymmetric MMs with artificially built-in threefold rotational symmetry and out-of-plane magnetization. Reflecting this particular symmetry and remanent zero-field magnetization, the direction and magnitude of spin-driven and potentially spin-polarized photocurrents are fully controlled without any external bias fields by tuning the polarization state of the excitation light. The spin-switchable nature of photocurrents under weak external magnetic fields allows for the additional functionality of spin current manipulation. Our experimental results, which are entirely consistent with symmetry predictions, show that nanoscale symmetry engineering can convert already known magnets into functional opto-spintronic materials working at room temperature.

Results

Magneto-photogalvanic effect and magnetic metamaterial design

The MPGE is a second-order nonlinear optical effect and can be phenomenologically expressed as^{13–15}

$$J_i = \beta_{ijk}^m(0; \omega, -\omega) E_j(\omega) E_k^*(\omega). \quad (1)$$

Here, $E_j(\omega)$ and $E_k^*(\omega) = E_k(-\omega)$ denote the j - and k -polarized electric fields, respectively, of the incident light wave at ω . These fields induce the i -directed zero-bias photocurrent J_i proportional to the square of the AC electric field; that is, to the intensity of the light. The third-rank polar tensor β_{ijk}^m changes the sign under either a time-reversal or space-inversion operation, and is determined by the magneto-crystalline symmetry of the system. Unlike the conventional (nonmagnetic) photogalvanic effect, in which the photocurrent direction reverses only under a space-inversion operation, the photocurrent driven by the MPGE reverses under both space-inversion and time-reversal operations. This makes the MPGE photocurrent in magnetic materials both spin-driven and spin-switchable¹⁵. A flexible nanostructure design not only elicits the second-order nonlinear optical effects in metamaterials²⁸, but also enables the manipulation of photo-driven ultrafast spin currents via the MPGE in properly designed MMs. This sophisticated manipulation is possible because the carriers in ferro- and ferri-magnetic materials carry a net spin angular momentum under an external DC electric field.

To demonstrate this novel artificially engineered opto-spintronic functionality, we designed a model MM system that generates polarization-controlled tunable directional spin-driven photocurrents (Fig. 1a). We fabricated the MM with a centrosymmetric Co/Pt ferro-magnetic metallic multilayer film with out-of-plane magnetization (Fig. 1b). It consists of periodic triangle-hole-arrayed nanostructures (antidot lattice) with threefold rotational symmetry. This particular

symmetry is necessary to control the direction and magnitude of zero-bias photocurrents due to angular momentum conservation in second-order nonlinear optical processes²⁸. The out-of-plane magnetization preserves the artificially built-in threefold rotational symmetry of the MM. Owing to the exchange splitting of the conduction band, carriers in the Co/Pt multilayer film are spin-polarized with an approximate polarization degree of 50%²⁹ (the ratio of spin-up and spin-down electron densities near the Fermi level is ~3:1).

When an arbitrarily polarized incident light (polarization angle θ_ω , ellipticity angle ε_ω) excites a MM with threefold rotational symmetry and out-of-plane magnetization M_z , zero-bias spin-driven photocurrents \mathbf{J}_m can be generated via the MPGE (Fig. 1a). Considering the magnetic point group of the MM as $3m'$ and assuming only one independent MPGE tensor component β^m , the magnitude $|\mathbf{J}_m|$ and flow direction θ_m of \mathbf{J}_m under $\pm M_z$ are respectively defined as³⁰

$$|\mathbf{J}_m| = |\beta^m| \cos 2\varepsilon_\omega \quad (-45^\circ \leq \varepsilon_\omega \leq 45^\circ), \quad (2)$$

$$\theta_m = \begin{cases} -2\theta_\omega \mp 90^\circ & (\beta^m > 0) \\ -2\theta_\omega \pm 90^\circ & (\beta^m < 0) \end{cases}, \quad (3)$$

where $|\mathbf{J}_m|$ and θ_m can be independently controlled by ε_ω and θ_ω of the excitation light, respectively (see Methods for a symmetry analysis). Figure 1c, d plot $|\mathbf{J}_m|$ and θ_m as functions of the polarization state of the excitation light, respectively, when $\beta^m > 0$. Note that reversing M_z does not change $|\mathbf{J}_m|$ but flips θ_m . Therefore, the direction and magnitude of the spin-driven photocurrents can be controlled and tuned, respectively, by controlling the polarization state of the excitation light. These relations are purely determined by the artificially built-in symmetry of the MM and (unlike the valley-dependent optical selection rules in transition metal dichalcogenides³¹) are not restricted to specific material properties or excitation wavelength.

Zero-bias spin-driven photocurrents

The MM was illuminated by a normal incident 800-nm femtosecond laser pulse (see Methods for experimental details). First, we measured the photocurrent J_x along the x direction across the unbiased MM with opposite out-of-plane saturation magnetization $\pm M_z$ under linearly y -polarized irradiation ($\theta_\omega = \varepsilon_\omega = 0^\circ$) (Fig. 2a). The magnitude of the detected zero-bias photocurrent scales linearly with light intensity (Fig. 2b). The light-to-current conversion ratio (~ 40 pA W⁻¹cm²) is similar to that obtained by the circular photogalvanic effect in Bi₂Se₃⁵, where spin-polarized photocurrents were induced by optically driving the Dirac cone with oblique-incidence circularly polarized light. In the present experiments, all helicity-dependent spin photocurrents, such as the spin-galvanic effect⁴ and circular photogalvanic effect⁵ are forbidden because the light is linearly polarized. In addition, the photocurrent observed here cannot be explained by the conventional (nonmagnetic) photogalvanic effect¹³ (see Supplementary Figs. 3, 4, 6 and Supplementary Discussion) or by the shift current mechanism^{32,33}. The photocurrent, whose direction is flipped by the time-reversal operation (reversal of M_z , Fig. 2b), can be explained only by the MPGE. We confirmed that the nonstructured centrosymmetric Co/Pt multilayer film do not generate zero-bias photocurrents for excitation light of any polarization.

The artificially built-in asymmetry in our MM imbalances the distribution of photoexcited carriers between the states with positive and negative wavevectors in the spin-up and spin-down subbands, causing electrons flows within each spin subband. As spin-up and spin-down electrons move in opposite directions through spin-dependent scattering, spin currents are generated^{11,12}. In a spin-polarized system, different populations of the two spin subbands yield a net electron flow. Thus, spin polarization of the zero-bias photocurrents can be detected as an electric current whose direction is switched by reversing M_z .

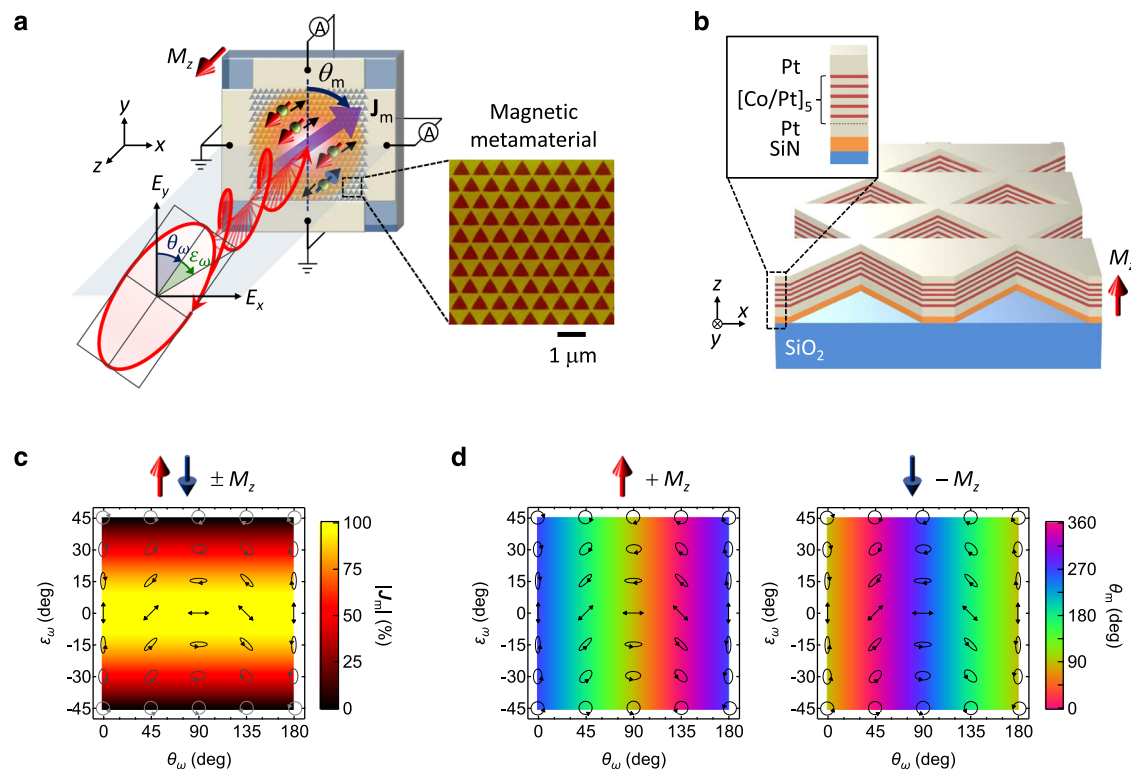


Fig. 1 | Polarization-controlled tunable directional spin-driven photocurrents in a magnetic metamaterial. **a** Schematic of the experimental setup for generating spin-driven photocurrents. A normally incident light with an arbitrarily polarized state (polarization angle θ_ω , ellipticity angle ϵ_ω) excites a magnetic metamaterial (MM) with threefold rotational symmetry and out-of-plane magnetization M_z , generating spin-driven photocurrents \mathbf{J}_m . The flow direction θ_m and magnitude $|\mathbf{J}_m|$ of \mathbf{J}_m can be independently controlled by θ_ω and ϵ_ω , respectively, via the magneto-photogalvanic effect. The inset shows an atomic force microscope image of the MM. **b** Schematic of the MM with a centrosymmetric Co/Pt ferromagnetic metallic

multilayer film, showing the direction of M_z . The MM consists of arrayed nanostructures (antidot lattice) of triangular holes with side lengths of 480 nm. The period of the triangular lattice is 558 nm. **c**, **d** 2D color maps of (c) $|\mathbf{J}_m|$ and (d) θ_m on the θ_ω vs ϵ_ω plane. The polarization states θ_ω and ϵ_ω of the excitation light are shown as black overlays. $|\mathbf{J}_m|$ can be modulated by ϵ_ω ($|\mathbf{J}_m| \propto \cos 2\epsilon_\omega$) for $\pm M_z$. Meanwhile, when $\beta^m > 0$, θ_m can be written as $\theta_m = -2\theta_\omega - 90^\circ$ for $+M_z$ (left panel) and $\theta_m = -2\theta_\omega + 90^\circ$ for $-M_z$ (right panel), leading to full-directional control by θ_ω . Reversal of M_z does not change $|\mathbf{J}_m|$ but flips θ_m , indicating direct coupling between the spin polarization direction and θ_m .

Time-resolved measurements reveal a sub-nanosecond response, although the rise- and fall-time responses are limited by the bandwidth of the instruments used in this experiment (Fig. 2c).

To clarify the coupling of the photocurrent to M_z , the magnetic-field dependence of J_x is plotted in Fig. 2d. The magnitude and sign of J_x suddenly change while sweeping the external out-of-plane magnetic field, yielding a ferromagnetic hysteresis with an antisymmetric closed loop. This behavior directly reflects spin polarization in the conduction band of the MM, as further evidenced by the measured magnetic-field dependence of the Faraday rotation θ_F (Fig. 2e). Therefore, the flow direction of the zero-bias photocurrents generated in our MM is directly coupled to the spin-polarization direction.

Full-directional control of the spin-driven photocurrents

To demonstrate the directional controllability of the spin-driven photocurrents, we rotated the polarization plane of the linearly polarized light ($\theta_\omega = 0^\circ - 360^\circ$, $\epsilon_\omega = 0^\circ$) and separately detected the photocurrents along the x and y directions (Fig. 3a). According to Eqs. (2) and (3), continuous rotation of θ_ω through 180° achieves full-directional control of \mathbf{J}_m with constant magnitude (Fig. 3b and c). When plotted against θ_ω , the spin-driven photocurrents $J_{m,x}$ and $J_{m,y}$ exhibits $-\cos 2\theta_\omega$ and $-\sin 2\theta_\omega$ behaviors, respectively (Fig. 3d). Reflecting the nearly identical amplitudes of $J_{m,x}$ and $J_{m,y}$, $|\mathbf{J}_m| (= \sqrt{J_{m,x}^2 + J_{m,y}^2})$ is almost independent of θ_ω (Fig. 3e). In contrast, $\theta_m (= \tan^{-1}(J_{m,x}/J_{m,y}))$ is a continuous function of θ_ω ; specifically, $\theta_m = -2\theta_\omega - 90^\circ$ (Fig. 3f). These behaviors are consistent with the above prediction. Overall, Fig. 3d-f demonstrate that by changing θ_ω of the linearly polarized

excitation light, spin-driven photocurrents with θ_ω -invariant magnitude can be directionally controlled through 360° in the two-dimensional (2D) plane of the MM. This is clearly different from the helicity-dependent bidirectional photocurrents observed in the Co/(nonmagnet)/Pt magnetic heterostructures³⁴.

Applying Eqs. (2) and (3), we further investigated whether a directional spin-driven photocurrent can be generated under an arbitrarily polarized light. For this purpose, we inserted a quarter-wave plate (QWP) after rotating the polarization angle φ_ω of the initially linearly polarized light, which modified both θ_ω and ϵ_ω of the excitation light (Fig. 4a). The polarization state of the excitation light is then determined by φ_ω and the rotation angle α of the QWP optical axis. In this setup, we can continuously modulate ϵ_ω with $\theta_\omega = 0^\circ/90^\circ$ at $\alpha = 0^\circ$ and $\theta_\omega = 45^\circ/135^\circ$ at $\alpha = 45^\circ$ (marked by the thick arrows in Fig. 4b, c, respectively), providing simultaneous control of $|\mathbf{J}_m|$ and θ_m .

To confirm this prediction, we investigated the spin-driven photocurrents $J_{m,x}$ and $J_{m,y}$ as functions of φ_ω . $J_{m,x}$ ($J_{m,y}$) shows $-\cos 2\varphi_\omega$ ($-\sin 2\varphi_\omega$) dependence on φ_ω whereas $J_{m,y}$ ($J_{m,x}$) is vanishingly small at $\alpha = 0^\circ$ ($\alpha = 45^\circ$) (upper (lower) panel of Fig. 4d). When plotted as a function of ϵ_ω , $|\mathbf{J}_m|$ exhibits the same behaviors at $\alpha = 0^\circ$ and 45° (Fig. 4e); specifically, $|\mathbf{J}_m| \propto \cos 2\epsilon_\omega$. Therefore, the magnitude can be tuned from 100% to 0% by switching from linear ($\epsilon_\omega = 0^\circ$) to circular ($\epsilon_\omega = \pm 45^\circ$) polarization. Meanwhile, θ_m can be independently controlled by θ_ω through the universal relation $\theta_m = -2\theta_\omega - 90^\circ$ at $\alpha = 0^\circ$ and 45° (Fig. 4e, inset), as observed under linearly polarized light (Fig. 3f). Thus, the polarization information of an arbitrarily polarized light is converted into the magnitude and flow direction of spin-driven photocurrents.

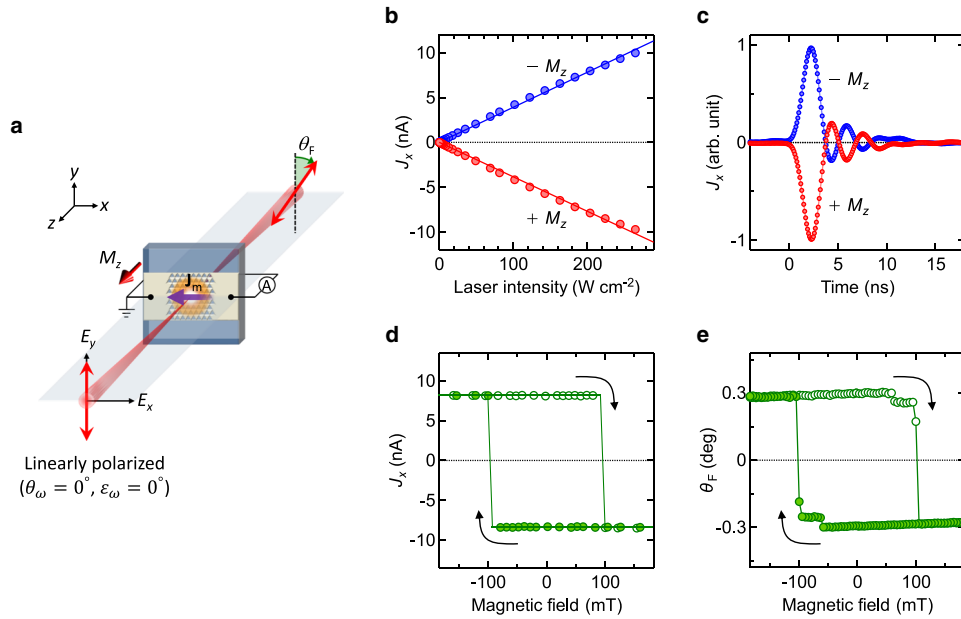


Fig. 2 | Fundamental properties of spin-driven photocurrents. **a** Schematic of the experimental setup for measuring zero-bias photocurrent J_x and Faraday rotation θ_F at normal incidence of linearly y-polarized ($\theta_\omega = \epsilon_\omega = 0^\circ$) 800 nm light. **b** Laser-intensity dependences of J_x for opposite out-of-plane saturation magnetizations $\pm M_z$. The lines are linearly fitted to the data. **c** Dynamical responses of J_x for $\pm M_z$. The response time is limited to the bandwidth of the instruments used. **d, e** Out-of-plane magnetic-field dependences of **(d)** J_x and **(e)** θ_F . The two-step

behaviors in θ_F arise from the experimental conditions: the incident laser beam hits not only the MM but also slightly the surrounding unstructured Co/Pt multilayer film with a smaller magnetic coercive field than that of the MM (see Supplementary Fig. 2). Two-step behavior is not observed in J_x in **(d)** because the unstructured Co/Pt multilayer film has a centrosymmetric structure and therefore does not contribute to the zero-bias photocurrent, which requires the breaking of space inversion symmetry.

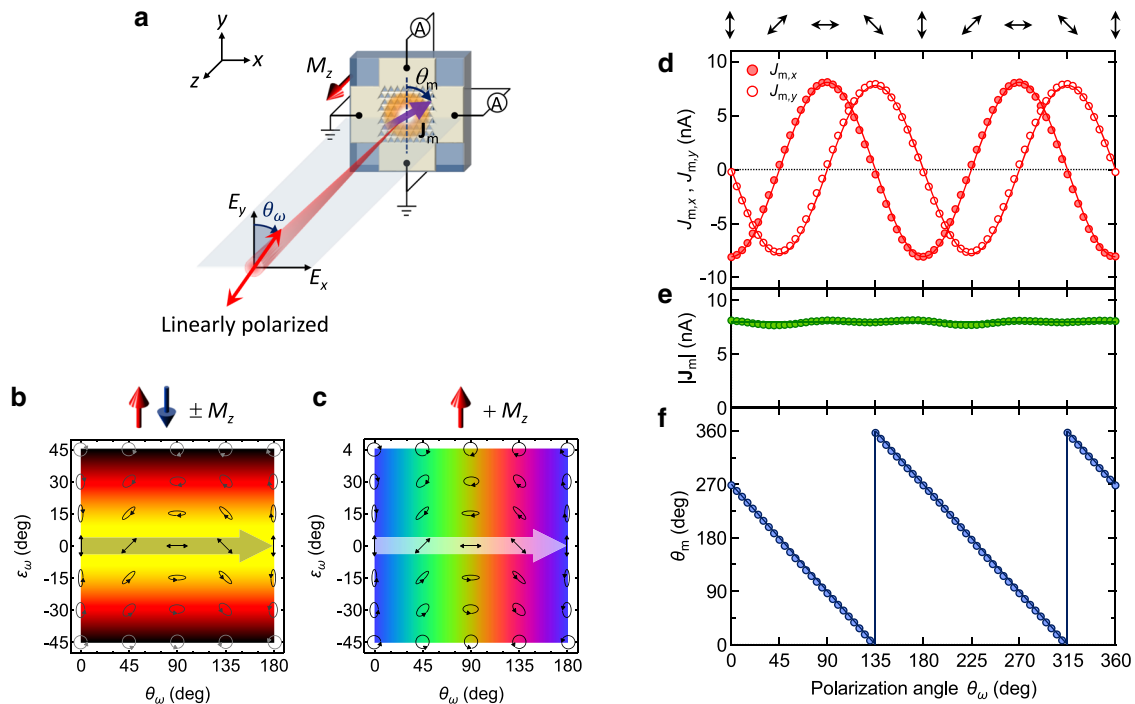


Fig. 3 | Full-directional control of spin-driven photocurrents. **a** Schematic of the experimental setup for measuring zero-bias photocurrents along the x and y directions at normal incidence of continuously rotated linearly polarized 800-nm light. **b, c** 2D color maps of **(b)** $|J_m|$ for $\pm M_z$ and **(c)** θ_m for $+ M_z$ when linearly polarized light crosses the horizontal directions (marked by thick arrows). **d** θ_ω dependence of $J_{m,x}$ and $J_{m,y}$, calculated as $J_{m,x} = [J_x(+M_z) - J_x(-M_z)]/2$ and

$J_{m,y} = [J_y(+M_z) - J_y(-M_z)]/2$, respectively, to exclude conventional (nonmagnetic) photogalvanic effects (see Supplementary Figs. 3, 4, 6 and Supplementary Discussion). The lines are fitted to $J_{m,x} \propto -\cos 2\theta_\omega$ and $J_{m,y} \propto -\sin 2\theta_\omega$. **e** $|J_m|$ calculated as $|J_m| = \sqrt{J_{m,x}^2 + J_{m,y}^2}$ and $|J_m| = \text{const}$. **f** θ_m calculated as $\theta_m = \tan^{-1}(J_{m,x}/J_{m,y})$ (blue circles) and fitted to $\theta_m = -2\theta_\omega - 90^\circ$ (blue lines).

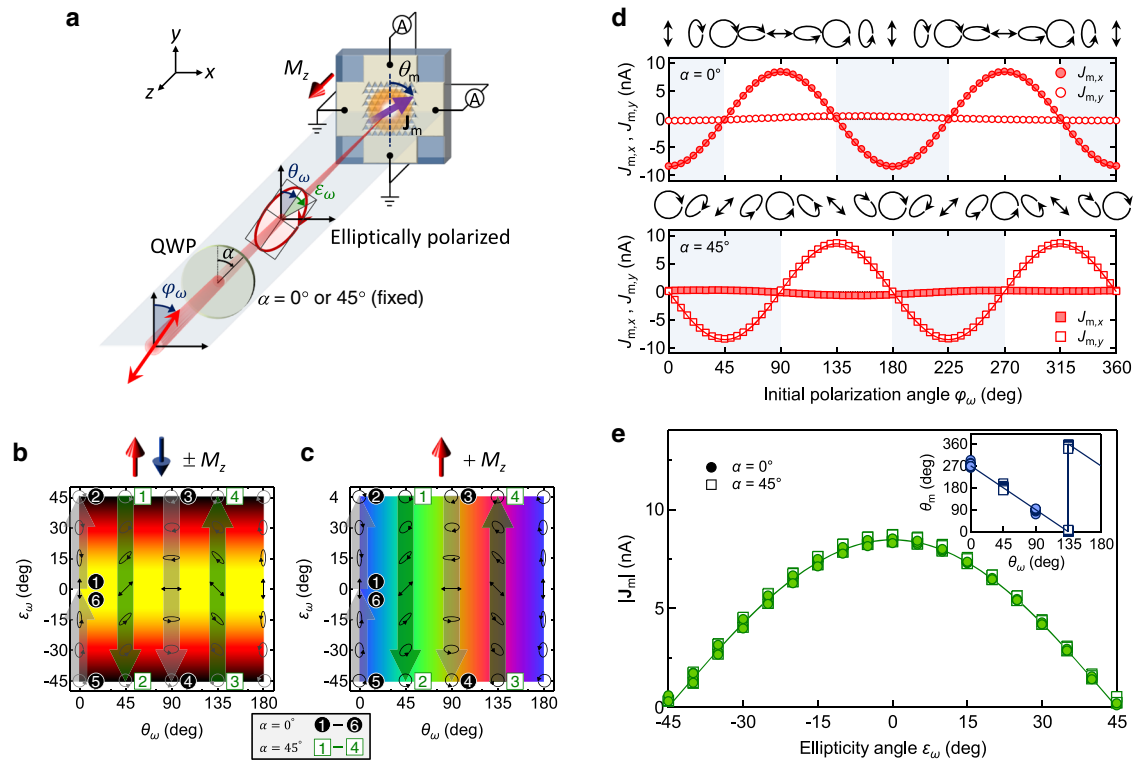


Fig. 4 | Simultaneous control of the magnitude and direction of spin-driven photocurrents. **a** Schematic showing the experimental setup for measuring zero-bias photocurrents along the *x* and *y* directions at normal incidence of continuously polarization-modulated 800-nm light. The polarization state of the excitation light is determined by the initial polarization angle φ_ω and rotation angle α of the optical axis of the quarter-wave plate (QWP). **b**, **c** 2D color maps of **(b)** $|J_m|$ for $\pm M_z$ and **(c)** θ_m for $+M_z$ when φ_ω crosses the vertical directions (marked by thick arrows). ε_ω can

be continuously modulated with $\theta_\omega = 0^\circ/90^\circ$ at $\alpha = 0^\circ$ and $\theta_\omega = 45^\circ/135^\circ$ at $\alpha = 45^\circ$, leading to the simultaneous control of $|J_m|$ and θ_m . **d** φ_ω dependence of $J_{m,x}$ and $J_{m,y}$ at $\alpha = 0^\circ$ (upper panel) and $\alpha = 45^\circ$ (lower panel). Shaded (nonshaded) areas correspond to $\theta_\omega = 0^\circ$ ($\theta_\omega = 90^\circ$) at $\alpha = 0^\circ$ and $\theta_\omega = 45^\circ$ ($\theta_\omega = 135^\circ$) at $\alpha = 45^\circ$. **e**, $|J_m| = \sqrt{J_{m,x}^2 + J_{m,y}^2}$ plotted as a function of ε_ω . The line is fitted to $|J_m| \propto \cos 2\varepsilon_\omega$. The inset plots $\theta_m = \tan^{-1}(J_{m,x}/J_{m,y})$ as a function of θ_ω . The line is fitted to $\theta_m = -2\theta_\omega - 90^\circ$.

Discussion

Based on microscopic calculations, we briefly explain the mechanism of photo-driven rectified charge and spin currents. Considering the dependence on the intensity of the excitation light, the experimentally observed light-induced DC current originates from the second-order photoelectric field, as is the case for the MPGE. The present MPGE can be attributed to the magnetic injection current¹⁵

$$\beta_{\mu\nu\lambda}^{\text{inj}} = \frac{-\pi q^3}{\gamma} \int \frac{d\mathbf{k}}{(2\pi)^2} \sum_{a \neq b} (v_{aa}^\mu - v_{bb}^\mu) g_{ab}^{\nu\lambda} \frac{\gamma}{\pi \gamma^2 + (\hbar\omega - E_b + E_a)^2} f(E_a) - f(E_b), \quad (4)$$

where q and γ are the elementary charge of carriers and the phenomenological scattering rate, respectively. $E_a(\mathbf{k})$ is the energy of one-particle, $f(x)$ is the Fermi-Dirac distribution function, v^μ is the velocity operator, and $g^{\nu\lambda}$ is the band-resolved quantum metric parametrized by the crystal momentum \mathbf{k} and band indices a and b ^{35,36}. The injection current arises from resonant excitation of the electron-hole pairs and shows a diverging behavior in clean materials. As our MM is a conductor, intraband dynamics may also contribute to the (magneto-)photogalvanic response to linearly polarized light³⁶. However, such intraband effects are expected to be negligible unless the frequency of light is as low as that of the THz waves³⁷. Additionally, we ignore the Fermi-surface contribution because the frequency of the irradiating light is comparable to the bandwidth (~ 1 eV)³⁸. The photogalvanic effect can be caused by the magnetic injection current only when the linearly polarized light is applied to systems where both space inversion and time-reversal symmetries are broken. These conditions are met by the MPGE discussed above.

In contrast, the spin photogalvanic effect (photo-driven rectified pure spin current) is formulated by calculating the spin current expectation value³⁶. In the paramagnetic state denoted by the magnetic point group $3m1'$, the dominant spin photogalvanic effect may occur due to the “spin” (linear) injection current denoted by

$$\tilde{\beta}_{\alpha\mu\nu\lambda}^{\text{Spinj}} = \frac{-\pi q^2}{\gamma} \int \frac{d\mathbf{k}}{(2\pi)^2} \sum_{a \neq b} (J_{aa}^{\alpha\mu} - J_{bb}^{\alpha\mu}) g_{ab}^{\nu\lambda} \frac{\gamma}{\pi \gamma^2 + (\hbar\omega - E_b + E_a)^2} f(E_a) - f(E_b), \quad (5)$$

which indicates the α -polarized spin current flow along the μ -direction under linearly polarized light. This formula is identical to that of the magnetic injection current (Eq. (4)) but with the velocity operator v^μ in Eq. (4) replaced with the spin current operator $J^{\mu\mu}$. The spin current operator is naively defined as $\{s^a, v^\mu\}/2$, where s^a is the spin operator. According to symmetry analysis, the allowed spin photogalvanic effect in the paramagnetic state is

$$\tilde{\beta}_{zx:xx} = -\tilde{\beta}_{zx:yy} = -\tilde{\beta}_{zy:xy} = -\tilde{\beta}_{zy:yx}, \quad (6)$$

for the *z*-polarized spin current and

$$\tilde{\beta}_{xy:xx} = -\tilde{\beta}_{xy:yy} = \tilde{\beta}_{yy:xy} = \tilde{\beta}_{yy:yx} = \tilde{\beta}_{yx:xx} = -\tilde{\beta}_{yx:yy} = -\tilde{\beta}_{xx:xy} = -\tilde{\beta}_{xx:yx}, \quad (7)$$

for the spin current whose polarization is in the *xy* plane.

Notably, the *z*-polarized spin current exhibits the same polarization dependence as the MPGE. This coincidence can be intuitively understood by the following arguments. The large exchange splitting (~ 1 eV) in ferromagnetic cobalt causes nonequivalence of the spin-up

and spin-down states. The photo-driven spin current is then converted into a strongly spin-polarized charge current, whereas the spin current carries no charge carriers in the paramagnetic state. Supporting this argument, both the z -polarized spin photocurrent and charge photocurrent follow the same polarization dependence originating from the same microscopic mechanism (namely, the injection mechanism). From these theoretical arguments on the experimental observations, the spin-polarized photocurrent is inferred to be controlled by the magnetic moment of the MM and the polarization state of the incident light.

The results of this proof-of-principle experiment newly demonstrate that nanoscale engineering of a standard spintronic thin film enables full manipulation of spin-driven photocurrents and can be applied to a broad range of ferro- and ferri-magnetic materials in general. The experimental results were entirely consistent with symmetry predictions, implying that our work can provide a guiding principle for the design and creation of artificially engineered opto-spintronic nanodevices and/or magnetic metasurfaces operating at room temperature. This study is complemented by ongoing successful explorations of novel magneto-optical and magnetoelectric functionalities in recently discovered 2D magnetic materials and heterostructures^{39,40}. Widely tunable nanostructures and highly spin-polarized materials such as half metals may generate intense spin-polarized photocurrents. Combining the potential for ultrafast photocurrent generation⁴¹ with propagation through materials with long spin diffusion lengths (such as graphene)⁴², efficient spin-polarized currents could be transferred into a ferromagnet. This approach can potentially control the magnetization direction via a spin-transfer torque on sub-picosecond timescales⁴³.

Our work can also guide the search for spin- and polarization-controllable THz devices and photovoltaic materials¹⁵. Recent studies have clarified the mechanisms of bulk photocurrent in magnetic systems and discussed applications for probing magnetic states^{35,36}. However, magnetic domain formation is a serious problem in bulk magnets. For instance, the photocurrent developed no hysteresis in ferromagnetic topological insulators⁶. In the present paper, the spin-driven photocurrents due to large exchange splitting were demonstrated in a controllable way without magnetic domain formation and surpassed the photocurrents of nonmagnetic origin (see Supplementary Fig. 6). Thus, MMs are an ideal platform for future studies and applications of photocurrent generation on magnetic materials.

Methods

Preparation of magnetic metamaterial

To incorporate novel opto-spintronic functionality into a standard ferromagnet, we fabricated a MM consisting of periodic triangle-hole-arrayed nanostructures (antidot lattice) with threefold rotational symmetry (Fig. 1b). Onto a two-sided polished SiO₂ substrate, we sequentially deposited a 5-nm-thick SiN layer, a 2-nm-thick Pt layer, a [Pt(0.9 nm)/Co(0.5 nm)]₅ ferromagnetic multilayer, and a 2-nm-thick Pt layer. The deposition was performed by radio-frequency magnetron sputtering. Subsequently, triangular holes were created by electron beam lithography over an area of 250 × 250 μm², followed by Ar ion etching. The side lengths of each triangular hole and the period of the triangular lattice were 480 nm and 558 nm, respectively, sufficiently shorter than the wavelength of the excitation light. The fabricated MM was evaluated by an atomic force microscope (Fig. 1a, inset). The single triangular hole structure belongs to point group $3m$, and its planar periodic array belongs to the $p3m1$ plane group with $3m$ point symmetry. At room temperature the Co/Pt ferromagnetic multilayer film exhibits out-of-plane magnetization that preserves the artificially built-in threefold rotational symmetry of the MM but breaks the time-reversal symmetry (the magnetic point group $3m'$). Thus, our MM breaks both the space inversion and time-reversal symmetries, providing the necessary condition for observing the MPGE.

Photocurrent measurements

To demonstrate the polarization-controlled tunable directional spin-driven photocurrents, the short-circuit photocurrents were measured across the unbiased MM (see Supplementary Fig. 1 for the device structure). The surrounding unstructured Co/Pt multilayer film was used as the electrodes. The excitation source was a Ti:sapphire ultrafast oscillator (Spectra-Physics, Mai Tai HP) operating at 690–1040 nm with a pulse width of 100 fs and a repetition rate of 80 MHz. The polarization state of the excitation light was controlled by a set of waveplates. A rotatable half-wave plate controlled the polarization angle θ_ω of the incident light and an optional QWP modulated the ellipticity angle ε_ω simultaneously with θ_ω (Fig. 4a). The MM was mounted in an electromagnet and its out-of-plane magnetization M_z was controlled by applying out-of-plane magnetic fields. The laser beam was delivered to the MM at normal incidence using an optical microscope. The spot delivered to the MM (~250 μm) was comparable in size to the nanostructured region. The laser power irradiated on the MM was typically ~100 mW, corresponding to a peak intensity of ~200 Wcm⁻². The laser beam passed through the MM to a charge-coupled device camera that monitored its position on the MM. The laser spot was carefully positioned at the center of the MM to exclude laser heating-induced thermoelectric currents such as the Seebeck effect⁵ and the anomalous Nernst effect⁴⁴. The intensity of the laser beam was modulated at f -1 kHz by an optical chopper. The short-circuit photocurrents were separately measured along the x and y directions by a two-phase lock-in amplifier (Stanford Research Systems, SR865) with the reference signal from the optical chopper. Thus, the photocurrent signals were evaluated as a time-averaged discharge current from the MM. The magnitude $|J_m|$ and flow direction θ_m of the spin-driven photocurrents were calculated as $|J_m| = \sqrt{(J_{m,x})^2 + (J_{m,y})^2}$ and $\theta_m = \tan^{-1}(J_{m,x}/J_{m,y})$, respectively.

The dynamical response of the photocurrents was measured with a digitizing storage oscilloscope (LeCroy, WaveRunner8104; bandwidth of 1 GHz) through a wide-band preamplifier (Stanford Research Systems, SR445A; bandwidth of 350 MHz). During the measurements, the MM was illuminated by a Ti:sapphire regenerative amplifier system (Spectra-Physics, Hurricane) operating at 800 nm with a pulse width of ~130 fs and a repetition rate of 1 kHz. The laser power irradiated on the MM was typically ~0.1 mW (~0.1 μJ/pulse). The time trace of the photocurrent was averaged 5000 times. The response was broadened by the response time of the preamplifier and was followed by oscillations (Fig. 2c) due to impedance mismatch in the circuit. All measurements were performed at room temperature in air.

Faraday rotation measurements

The magnetization curves of the unstructured Co/Pt multilayer film and MM were evaluated using Faraday rotation measurements under the 800 nm laser light used for the photocurrent measurements (see Fig. 2e and Supplementary Fig. 2). Due to the Faraday effect, the plane of the linearly polarized light rotates after passing through the magnetic materials. The Faraday rotation angle θ_F , measured using a conventional balanced detection technique, is proportional to M_z .

Linear optical measurements

The linear transmittance (T) and reflectivity (R) spectra of the unstructured Co/Pt multilayer film and MM were measured over the 250–2500 nm range using a commercial spectrometer (JASCO, MSV-5200). The absorption (A) spectra were calculated as $A = 1 - T - R$ (see Supplementary Fig. 5).

Symmetry analysis of the magneto-photogalvanic effect

Under the magnetic point group of $3m'$ for the MM with a spontaneous magnetization parallel to the threefold rotational axis, the MPGE has four independent nonzero tensor components³⁰:

$\beta_{xxx}^m = -\beta_{xyy}^m = -\beta_{yyx}^m = -\beta_{yxx}^m \equiv \beta^m$, $\beta_{xyz}^m = -\beta_{yxz}^m$, $\beta_{xzy}^m = -\beta_{yzx}^m$, $\beta_{zxy}^m = -\beta_{zyx}^m$. When a laser light $\mathbf{E}(\omega) = \mathbf{E}_0 e^{-i(kz - \omega t)}$ propagating along the $-z$ direction is irradiated on the MM at normal incidence (Fig. 1a), only β^m contributes to the spin-driven photocurrents in the 2D plane of the MM. Under arbitrarily polarized light irradiation with $\mathbf{E}_0 = (E_x, E_y, E_z) = (\sin \theta_\omega \cos \varepsilon_\omega - i \cos \theta_\omega \sin \varepsilon_\omega, \cos \theta_\omega \cos \varepsilon_\omega + i \sin \theta_\omega \sin \varepsilon_\omega, 0)$, spin-driven photocurrents are generated along the x and y directions as

$$J_{m,x} = \beta^m (E_x E_x^* - E_y E_y^*) = -\beta^m \cos 2\theta_\omega \cos 2\varepsilon_\omega, \quad (8)$$

$$J_{m,y} = -\beta^m (E_x E_y^* + E_y E_x^*) = -\beta^m \sin 2\theta_\omega \cos 2\varepsilon_\omega. \quad (9)$$

From these expressions, we get

$$|J_m| = \sqrt{(J_{m,x})^2 + (J_{m,y})^2} = |\beta^m| \cos 2\varepsilon_\omega \quad (-45^\circ \leq \varepsilon_\omega \leq 45^\circ), \quad (10)$$

and

$$\theta_m = \begin{cases} -2\theta_\omega \mp 90^\circ & (\beta^m > 0) \\ -2\theta_\omega \pm 90^\circ & (\beta^m < 0) \end{cases} \quad (11)$$

where \mp and \pm in Eq. (11) depends on the magnetization direction $\pm M_z$. Equations (10) and (11) imply that $|J_m|$ and θ_m of the spin-driven photocurrents can be independently controlled by ε_ω and θ_ω of the excitation light, respectively, and that θ_m flips when M_z reverses. Thus, the polarization information of an arbitrarily polarized light can be converted into the magnitude and flow direction of the spin-driven photocurrents. These relations are purely determined by the artificially built-in symmetry of the MM and are not restricted to specific material properties or excitation wavelength³¹, thus allowing broad-band operation (see Supplementary Fig. 6). The conventional (nonmagnetic) photogalvanic effect is discussed in Supplementary Figs. 3, 4, 6 and Supplementary Discussion.

Data availability

The data that support the findings of this study are available from the corresponding author upon reasonable request.

References

- Wolf, S. A. et al. Spintronics: a spin-based electronics vision for the future. *Science* **294**, 1488–1495 (2001).
- Žutić, I., Fabian, J. & DasSarma, S. Spintronics: fundamentals and applications. *Rev. Mod. Phys.* **76**, 323–410 (2004).
- Maekawa, S., Saitoh, E., Valenzuela, S. O. & Kimura, T. *Spin Current* (Oxford University Press, Oxford, U.K., 2012).
- Ganichev, S. D. et al. Spin-galvanic effect. *Nature* **417**, 153–156 (2002).
- McIver, J. W., Hsieh, D., Steinberg, H., Jarillo-Herrero, P. & Gedik, N. Control over topological insulator photocurrents with light polarization. *Nat. Nanotech.* **7**, 96–100 (2012).
- Ogawa, N. et al. Zero-bias photocurrent in ferromagnetic topological insulator. *Nat. Commun.* **7**, 12246 (2016).
- Rudolf, D. et al. Ultrafast magnetization enhancement in metallic multilayers driven by superdiffusive spin current. *Nat. Commun.* **3**, 1037 (2012).
- Satoh, T. et al. Directional control of spin-wave emission by spatially shaped light. *Nat. Photon.* **6**, 662–666 (2012).
- Zhao, H., Loren, E. J., van Driel, H. M. & Smirl, A. L. Coherence control of Hall charge and spin currents. *Phys. Rev. Lett.* **96**, 246601 (2006).
- Uchida, K. et al. Generation of spin currents by surface plasmon resonance. *Nat. Commun.* **6**, 5910 (2015).
- Ganichev, S. D. et al. Zero-bias spin separation. *Nat. Phys.* **2**, 609–613 (2006).
- Ganichev, S. D. et al. Spin currents in diluted magnetic semiconductors. *Phys. Rev. Lett.* **102**, 156602 (2009).
- Sturman, B. I. & Fridkin, V. M. *The Photovoltaic and Photoconductive Effects in Noncentrosymmetric Materials* (Gordon and Breach Science Publishers, 1992).
- Bel'kov, V. V. et al. Magneto-gyrotropic photogalvanic effects in semiconductor quantum wells. *J. Phys.: Condens. Matter* **17**, 3405–3428 (2005).
- Zhang, Y. et al. Switchable magnetic bulk photovoltaic effect in the two-dimensional magnet CrI₃. *Nat. Commun.* **10**, 3783 (2019).
- Soukoulis, C. M. & Wegener, M. Past achievements and future challenges in the development of three-dimensional photonic metamaterials. *Nat. Photon.* **5**, 523–530 (2011).
- Shelby, R. A., Smith, D. R. & Schultz, S. Experimental verification of a negative index of refraction. *Science* **292**, 77–79 (2001).
- Pendry, J. B. Negative refraction makes a perfect lens. *Phys. Rev. Lett.* **85**, 3966–3969 (2000).
- Pendry, J. B., Schurig, D. & Smith, D. R. Controlling electromagnetic fields. *Science* **312**, 1780–1782 (2006).
- Landy, N. I., Sajuyigbe, S., Mock, J. J., Smith, D. R. & Padilla, W. J. Perfect metamaterial absorber. *Phys. Rev. Lett.* **100**, 207402 (2008).
- Kauranen, M. & Zayats, A. V. Nonlinear plasmonics. *Nat. Photon.* **6**, 737–748 (2012).
- Lorke, A. et al. Far-infrared and transport properties of antidot arrays with broken symmetry. *Physica B* **249–251**, 312–316 (1998).
- Valev, V. K. et al. Plasmons reveal the direction of magnetization in nickel nanostructures. *ACS Nano* **5**, 91–96 (2011).
- Sekine, D., Sato, Y. & Matsubara, M. Nonlinear optical detection of mesoscopic magnetic toroidal dipoles. *Appl. Phys. Lett.* **120**, 162905 (2022).
- Kida, N. et al. Optical magnetoelectric effect in a submicron patterned magnet. *Phys. Rev. Lett.* **94**, 077205 (2005).
- Faltermeier, P. et al. Magnetic quantum ratchet effect in (Cd,Mn)Te- and CdTe-based quantum well structures with a lateral asymmetric superlattice. *Phys. Rev. B* **95**, 155442 (2017).
- Faltermeier, P. et al. Circular and linear magnetic quantum ratchet effects in dual-grating-gate CdTe-based nanostructures. *Physica E* **101**, 178–187 (2018).
- Konishi, K. et al. Polarization-controlled circular second-harmonic generation from metal hole arrays with threefold rotational symmetry. *Phys. Rev. Lett.* **112**, 135502 (2014).
- Rajanikanth, A., Kasai, S., Ohshima, N. & Hono, K. Spin polarization of currents in Co/Pt multilayer and Co-Pt alloy thin films. *Appl. Phys. Lett.* **97**, 022505 (2010).
- Birss, R. R. *Symmetry and Magnetism*, (North-Holland, Amsterdam, 1966).
- Xie, L. & Cuia, X. Manipulating spin-polarized photocurrents in 2D transition metal dichalcogenides. *PNAS* **113**, 3746–3750 (2016).
- Belinicher, V. I., Ivchenko, E. L. & Sturman, B. I. Kinetic theory of the displacement photovoltaic effect in piezoelectrics. *Sov. Phys. JETP* **56**, 359–366 (1982).
- Young, S. M. & Rappe, A. M. First principles calculation of the shift current photovoltaic effect in ferroelectrics. *Phys. Rev. Lett.* **109**, 116601–223 (2012).
- Li, G. et al. Laser induced THz emission from femtosecond photocurrents in Co/ZnO/Pt and Co/Cu/Pt multilayers. *J. Phys. D: Appl. Phys.* **51**, 134001 (2018).
- Ahn, J., Guo, G. & Nagaosa, N. Low-frequency divergence and quantum geometry of the bulk photovoltaic effect in topological semimetals. *Phys. Rev. X* **10**, 041041 (2020).
- Watanabe, H. & Yanase, Y. Chiral photocurrent in parity-violating magnet and enhanced response in topological antiferromagnet. *Phys. Rev. X* **11**, 011001 (2021).

37. Plank, H. et al. Infrared/terahertz spectra of the photogalvanic effect in (Bi,Sb)Te based three-dimensional topological insulators. *Phys. Rev. Mater* **2**, 024202 (2018).
38. Ebert, H., Ruegg, S., Schuetz, G., Wienke, R. & Zeper, W. B. Magnetic properties of Co/Pt-multilayers. *J. Magn. Magn. Mater.* **93**, 601–604 (1991).
39. Gong, C. & Zhang, X. Two-dimensional magnetic crystals and emergent heterostructure devices. *Science* **363**, 706 (2019).
40. Gibertini, M., Koperski, M., Morpurgo, A. F. & Novoselov, K. S. Magnetic 2D materials and heterostructures. *Nat. Nanotech.* **14**, 408–419 (2019).
41. Braun, L. et al. Ultrafast photocurrents at the surface of the three-dimensional topological insulator Bi₂Se₃. *Nat. Commun.* **7**, 13259 (2016).
42. Cha, S. et al. Generation, transport and detection of valley-locked spin photocurrent in WSe₂-graphene-Bi₂Se₃ heterostructures. *Nat. Nanotech.* **13**, 910 (2018).
43. Schellekens, A. J., Kuiper, K. C., de Wit, R. R. J. C. & Koopmans, B. Ultrafast spin-transfer torque driven by femtosecond pulsed-laser excitation. *Nat. Commun.* **5**, 4333 (2014).
44. Weiler, M. et al. Local charge and spin currents in magnetothermal landscapes. *Phys. Rev. Lett.* **108**, 106602 (2012).

Acknowledgements

M.M. thanks M. Shigefuji and D. Sekine for technical support, and T. Ishihara for useful comments. This work was supported by JSPS KAKENHI (Grant Nos. 21H04649, 22K18962, 17H04844, and 16K13658), the Mitsubishi Foundation, the Research Foundation for Opto-Science and Technology, the Support Center for Advanced Telecommunications Technology Research Foundation, the Murata Science Foundation, the Noguchi Institute, the Research Foundation for the Electrotechnology of Chubu, the SEI Group CSR Foundation, the Inamori Foundation, the Kato Foundation for Promotion of Science, the Iketani Science and Technology Foundation, the Izumi Science and Technology Foundation, the Mayekawa Houonkai Foundation, the Asahi Glass Foundation, the Nippon Sheet Glass Foundation for Materials Science and Engineering, the Intelligent Cosmos Academic Foundation, the Foundation for Promotion of Material Science and Technology of Japan, the Konica Minolta Science and Technology Foundation, the Sumitomo Foundation, the Yamaguchi Educational and Scholarship Foundation, and the Tanaka Memorial Foundation. A part of this work was conducted at Nagoya University, supported by the “Nanotechnology Platform Program” of the Ministry of Education, Culture, Sports, Science and Technology, Japan (Grant No. JPMXP09F17NU0108).

Author contributions

M.M. designed and coordinated the study contributed to all measurements and calculations, and wrote the manuscript. T.Ko. carried out the photocurrent measurements and analyzed the data. T.Ka. and S.I. fabricated the magnetic metamaterials. H.W. and Y.Y. theoretically interpreted the microscopic origin and contributed to the writing of the paper. All authors commented on the manuscript.

Competing interests

The authors declare no competing interests.

Additional information

Supplementary information The online version contains supplementary material available at <https://doi.org/10.1038/s41467-022-34374-7>.

Correspondence and requests for materials should be addressed to Masakazu Matsubara.

Peer review information *Nature Communications* thanks Ranjan Singh and the other, anonymous, reviewer(s) for their contribution to the peer review of this work.

Reprints and permissions information is available at <http://www.nature.com/reprints>

Publisher’s note Springer Nature remains neutral with regard to jurisdictional claims in published maps and institutional affiliations.

Open Access This article is licensed under a Creative Commons Attribution 4.0 International License, which permits use, sharing, adaptation, distribution and reproduction in any medium or format, as long as you give appropriate credit to the original author(s) and the source, provide a link to the Creative Commons license, and indicate if changes were made. The images or other third party material in this article are included in the article’s Creative Commons license, unless indicated otherwise in a credit line to the material. If material is not included in the article’s Creative Commons license and your intended use is not permitted by statutory regulation or exceeds the permitted use, you will need to obtain permission directly from the copyright holder. To view a copy of this license, visit <http://creativecommons.org/licenses/by/4.0/>.

© The Author(s) 2022